Journal of Molecular Liquids 308 (2020) 113040

Contents lists available at ScienceDirect

Journal of Molecular Liquids

journal homepage: www.elsevier.com/locate/molliq

A way to introducing a hydrophilic bioactive agent into model lipid membranes. The role of cetyl palmitate in the interaction of curcumin with 1,2-dioleoyl-*sn*-glycero-3-phosphatidylcholine monolayers

Maxime Girardon [a], Beata Korchowiec [b,*], Jacek Korchowiec [b], Ewa Rogalska [a,*], Nadia Canilho [a], Andreea Pasc [a]

[a] Laboratoire Lorrain de Chimie Moléculaire (L2CM) UMR 7053, Université de Lorraine-FST, Boulevard des Aiguillettes, 54506 Vandoeuvre-Lès-Nancy, France
[b] Faculty of Chemistry, Jagiellonian University, ul. Gronostajowa 2, 30-387 Krakow, Poland

ARTICLE INFO

Article history:
Received 7 February 2020
Received in revised form 24 March 2020
Accepted 31 March 2020
Available online 02 April 2020

Keywords:
Molecular modeling
Miscibility in monomolecular films
Thermodynamics
Model cell membrane
DOPC
Cetyl palmitate
Curcumin
PM-IRRAS

ABSTRACT

The interfacial behavior of curcumin, a model anti-inflammatory drug was studied upon interaction with cetyl palmitate and 1,2-dioleoyl-*sn*-glycero-3-phosphatidylcholine. Cetyl palmitate finds applications for topical delivery in nanostructured lipid carriers, while the phosphatidylcholine was used both as a component of the carrier and as a model membrane lipid. Here, surface pressure, thermodynamics, Brewster angle microscopy, molecular dynamics and polarization modulation infrared reflection-absorption spectroscopy were used to better our understanding of the interaction between the components of the delivery systems and, on the other hand, of their interaction with biological membranes. Moreover, thermodynamics was used to analyze the effect of curcumin on the lipid systems and, in particular, on the model membranes. The results obtained indicate that mixtures of curcumin and cetyl palmitate form Langmuir films, while none of the two pure components does. This effect was interpreted in terms of formation of a complex between curcumin and the hydrophobic, water insoluble cetyl palmitate. The hydrophilic-hydrophobic balance of the complex allows its penetration into the monolayer and mixing with the phospholipid phase. This finding may be of interest for further design of phytolipids for drug delivery applications.

1. Introduction

Curcumin (CC), a diarylheptanoid of plant origin finds applications in food and cosmetics, and new developments in the medicinal chemistry are described in the literature [1]. Clinical and preclinical studies indicate that curcumin may have several health benefits due to its antioxidant, antimicrobial and anti-inflammatory activity, or even anticancer potential when used as a dietary supplement. Recent studies also suggested beneficial effects of curcumin in degenerative diseases such as Alzheimer, type II diabetes and Parkinson [2]. However, curcumin has low bioavailability as it is poorly soluble in physiological conditions ($<3\ mg \cdot L^{-1}$) and poorly absorbed. Moreover, it is rapidly metabolized and eliminated [3,4]. High administration doses are usually needed to observe any *in vivo* effect whatever the administration route. Consequently, encapsulation of CC is proposed to improve its bioavailability. Different delivery systems of CC such as liposomes [5,6], self-microemulsified drug delivery systems [7], solid or nanostructured lipid particles [8,9], polymeric nanoparticle [10], silica based materials such as hollow mesoporous microspheres [11] or hybrid meso-macrostructured silica containing curcumin-loaded solid lipid macrocavities [12,13] were developed to date. Among them, solid lipid nanoparticles (SLN) appear to be the most promising since they combine the advantages of biocompatible and biodegradable lipid matrix, an increase of drug stability and bioavailability, a sustained and controlled drug release and possibility of large-scale production without organic solvents. The delicate point is that the drug loading capacity of conventional SLN is limited by the solubility of drug in the lipid matrix. Since incorporated drugs are located between fatty acid chains, between the lipid layers and also in crystal imperfections, a highly ordered crystal lattice cannot accommodate large amounts of drug. Therefore, the use of more complex lipids is more practical for higher drug loading [14]. Another important point to be taken into account when developing SLN-based delivery systems is interaction between the particles and cell membranes [15]. To address all these problems, *i.e.* the interaction between all SLN constituents and, on the other hand, their interaction with membranes, Langmuir film technique can be employed. Indeed,

* Corresponding authors.
E-mail addresses: bkorch@chemia.uj.edu.pl (B. Korchowiec), ewa.rogalska@univ-lorraine.fr (E. Rogalska).

https://doi.org/10.1016/j.molliq.2020.113040

the Langmuir technique [16] offers an easy way to prepare model membranes and to study the interaction of lipid monolayers with third molecules [17–23]. Importantly, Langmuir films can be prepared with the amphiphilic molecules forming the SLNs. This approach can be useful for a better understanding of the parameters which are decisive both for the structure and properties of the SLNs and for their impact on the lipid membrane.

Here, the interaction of the SLN and membrane constitutive molecules was investigated using Langmuir compression isotherms, Brewster angle microscopy (BAM) and polarization modulation infrared reflection-absorption spectroscopy (PM-IRRAS), thermodynamic analysis, and molecular modeling. We demonstrate that 1,2-dioleoyl-*sn*-glycero-3-phosphatidylcholine (DOPC) enhances the solubility of curcumin in the solid phase of a fatty ester, cetyl palmitate (CP) [24]. Our results elucidate the mechanism of this effect, which is based on the polar and apolar interaction between curcumin and cetyl palmitate followed by a further interaction of these adducts with DOPC.

2. Materials and methods

2.1. Materials and reagents

Synthetic 1,2-dioleoyl-*sn*-glycero-3-phosphocholine (DOPC, >99% pure) was purchased from Avanti Polar Lipids. Curcumin (≥99.5%), cetyl palmitate (≥99%), were from Sigma-Aldrich. Chloroform (99.9% pure) was from Biosolve. Curcumin (CC), cetyl palmitate (CP) and DOPC were dissolved in chloroform to reach a final concentration of 0.5–1.0 $mg \cdot mL^{-1}$. The stock solutions of CC and CP were used to prepare 1:1 M ratio CP/CC mixture. Tri-components mixtures were prepared at various molar ratios from stock solutions of DOPC and 1:1 CP/CC. The stock solutions were stored at −18 °C. All subphases were prepared with pure Milli-Q water (Millipore), resistivity 18 MΩ cm, surface tension of 72.8 $mN \cdot m^{-1}$ at 20 °C. Molecular structures of the compounds used in this study are presented in Fig. 1.

2.2. Compression isotherms

The surface pressure - area (Π-A) isotherms were recorded with a KSV 2000 Langmuir balance (KSV Instruments, Helsinki). The isotherms were measured for pure compound monolayers, as well as their mixtures. The surface pressure was monitored using a platinum Wilhelmy plate. The thermostated Teflon® trough of the effective film area of 377 cm^2 was equipped with two hydrophilic Delrin® barriers (symmetric compression). Before each measurement, the water subphase surface was cleaned by sweeping and suction. Next the film was spread on the subphase. The solutions were spread with a Hamilton syringe on the free water surface and left for 15 min to allow solvent evaporation and to reach an equilibrium state of the monolayer. All isotherms were recorded upon symmetric compression of the monolayer at a constant barrier speed of 5 $mm \cdot min^{-1}$. In the case of binary or ternary mixtures, the surface pressure was plotted against the mean molecular area, obtained by dividing the total surface area by the number of molecules spread on the surface. For each monolayer composition, measurements were repeated at least 3 times. The Π-A isotherms were recorded at 18, 25 and 32 ± 0.1 °C. The standard deviation obtained from compression isotherms was ±0.5 $Å^2$ on molecular area and ± 0.2 $mN \cdot m^{-1}$ on surface pressure.

The compression isotherms allowed determining the compressibility modulus, C_S^{-1}, [25] as:

$$C_S^{-1} = -A(\partial \Pi / \partial A)_T \quad (1)$$

2.3. Thermodynamic analysis

The Gibbs energy of mixing, ΔG^{mix}, was calculated from Π-A isotherms using the following formula:

$$\Delta G^{mix} = \int_0^{\Pi} [A_{12} - (x_1 A_1 + x_2 A_2)] d\Pi \quad (2)$$

$$\Delta G^{mix} = \int_0^{\Pi} [A_{123} - (x_1 + x_2) A_{12} - x_3 A_3] d\Pi \quad (3)$$

where A_{12} is the mean molecular area in the mixed monolayer at a given surface pressure, A_1 and A_2 are the mean molecular areas of the pure components 1 and 2 at the same surface pressure, and x_1 and x_2 are the mole fractions of the two compounds in the mixed film [26,27]. The thermodynamic terms used here were defined in our previous papers [28,29]. Namely, in accordance with the definition of Gibbs energy of mixing, $\Delta G^{mix} = G - (x_1 G_1 + x_2 G_2)$, Eq. (2) gives ΔG^{mix} instead of ΔG^{exc} given by F. C. Goodrich et al. [26] and K. J. Bacon et al. [27].

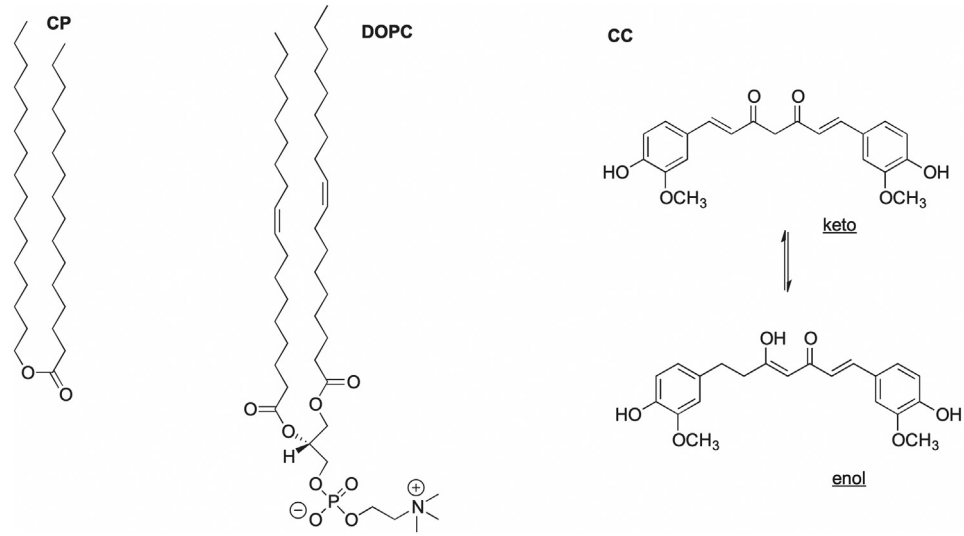

Fig. 1. Molecular structures of cetyl palmitate (CP), 1,2-dioleoyl-*sn*-glycero-3-phosphocholine (DOPC) and curcumin (CC) tautomers (keto and enol).

2.4. Brewster angle microscopy

The morphology of the films was imaged with a computer-interfaced KSV 2000 Langmuir balance combined with a Brewster angle microscope (KSV Optrel BAM 300, Helsinki). The Teflon® trough dimensions were 58 × 6.5 × 1 cm; other experimental conditions were as described above.

2.5. Polarization-modulation infrared reflection-absorption spectroscopy (PM-IRRAS)

The PM-IRRAS spectra [30] of DOPC and all mixed DOPC/CP/CC monolayers spread on pure water subphase were acquired at 25 °C. The Teflon® trough dimensions were 36.5 × 7.5 × 0.5 cm; other experimental conditions were as described in the preceding paragraph. The PM-IRRAS measurements were performed using a KSV PMI 550 instrument (KSV Instruments Ltd., Helsinki, Finland). The PMI 550 contains a compact Fourier Transform IR-spectrometer equipped with a polarization-modulation (PM) unit on one arm of a goniometer, and a MCT-detector on the other arm. The incident angle of the light beam can be freely chosen between 40° and 90°; here, the incident angle was 79°. The spectrometer and the PM-unit operate at different frequencies, allowing separation of the two signals at the detector. The PM unit consists of a photoelastic modulator, which is an IR-transparent, ZnSe piezoelectric lens. The incoming light is continuously modulated between *s*- and *p*- polarization at a frequency of 74 kHz. This allows simultaneous measurement of spectra for the two polarizations, the difference providing surface specific information, and the sum providing the reference spectrum. As the spectra are measured simultaneously, the effect of water vapor is largely reduced. The PM-IRRAS spectra of the film-covered surface, S(f), as well as that of the pure water, S(w), were measured and the normalized difference $\Delta S/S = [S(f) - S(w)] / S(w)$ is reported. 6000 interferogram scans (10 scans per second) have been acquired for each spectrum. In the mid-IR region, the wavenumber at which the half-wave retardation takes place can be freely selected. Here, the maximum of PEM efficiency was set either to 1500 or to 2900 cm^{-1} for analyzing the carbonyl stretching or methylene stretching regions of the spectra, respectively. The spectral range of the device is 800–4000 cm^{-1} and the resolution is 8 cm^{-1}.

2.6. Molecular modeling

The geometric structures of curcumin in keto and enol forms located at B3LYP/6-311G(d,p) level of theory are depicted in Fig. 2. Grimme dispersion correction was taken into account [31]. All calculations were done using Gaussian 09 suit of programs [32]. The enol form (Fig. 2A) is planar and is slightly more stable than the keto form (Fig. 2B). Free enthalpy of enol form ($T = 293$ K and $p = 1$ bar) is lower by 4 kcal mol^{-1}. The higher stabilization can be attributed to π-conjugation effect and the formation of hydrogen-bond in the central part of the molecule (Fig. 2A). The keto form is more flexible compared to the enol form (rotation involving bonds of the central -CH_2- group). Both structures were taken to derive the CHARMM force field parameters [33]. The procedure described in reference [34] was utilized (MP2/6-31G(d) level of theory). The derived parameters were checked in the explicit solvent type calculations (enol and keto forms of curcumin in a water box). The molecular dynamics (MD) simulations allowed to locate two additional conformers of the keto form (Fig. 3). Both structures were reoptimized at B3LYP/6-311(d,p) level of theory. Among the keto forms, the stack conformer is the most stable in vacuum, however, still less stable than enol form (B3LYP/6-311G**). Free enthalpy of the enol form is 2 kcal mol^{-1} lower than the keto form ($T = 293$ K and $p = 1$ bar). The polarizable continuum model [35] indicates that the keto conformer shown in Fig. 2B is the most stable in solution. The equilibrium between the keto and enol isomers in solution depends on the environment (pH, solvent type, temperature).

The MD setup applied in this study consists of two monolayers spread on the opposite sides of the water slab. Each monolayer is built of 100 molecules distributed on a 2-dimensional grid. The rotation of each molecule around the *z*-axis was random. In a two-components monolayer, the molecules were at equimolarity and were chosen randomly. The headgroups of DOPC and CP were immersed in water while the hydrophobic tails were directed towards vacuum. The DOPC, CP, DOPC/CP, DOPC/CC and CP/CC systems were considered. Calculations for enol and keto isomers of CC were performed separately.

Molecular dynamics simulations were performed with NAMD program [36]. All-atom CHARMM36 force field was applied [33]. The TIP3P model was assumed for water molecules [37]. Langevin thermostat and barostat were used to control the temperature and pressure. Van der Waals interactions were switched off at 12 Å. Electrostatic energy was calculated with the PME method. A 1 fs time step was used in all simulations. The calculations were performed with periodic boundary conditions imposed on the system. The initial size of the box in the *z*-direction was 1000 Å. Translational replicas in this direction were separated by a vacuum slab in order to minimize long-range electrostatic interactions. All molecular systems were minimized. The initial simulations were carried out in a canonical ensemble for 5 ns. The final simulations were carried out at constant temperature ($T = 293$ K), normal pressure ($p_n = 1$ bar), and surface tension ($\gamma = 20$ mN m^{-1}). The (N, T, p_n, γ) simulations were equilibrated for 40 ns. The data were computed using 10 ns production runs. Trajectories were visualized with VMD package [38].

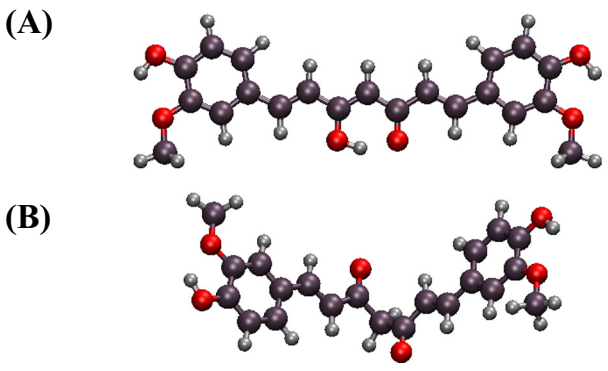

Fig. 2. Schematic view of enol (A) and keto (B) forms of curcumin as located at B3LYP/6-311G(d,p) level of theory.

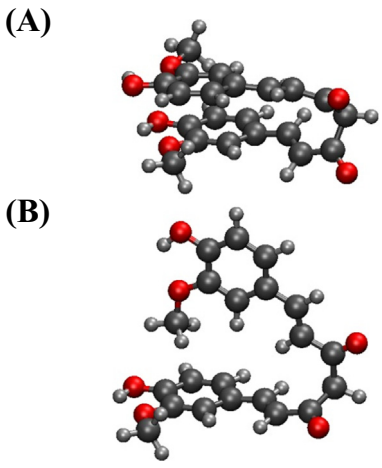

Fig. 3. Schematic view of stack (A) and internal T-shape (B) conformers of keto form of CC as located at B3LYP/6-311G(d,p) level of theory.

3. Results and discussion

3.1. Compression isotherms and Brewster angle microscopy of pure and mixed films

The interfacial behavior of curcumin, cetyl palmitate, 1,2-dioleoyl-*sn*-glycero-3-phosphocholine and their mixtures was studied using Langmuir film technique. The obtained surface pressure - area (Π-A) isotherms of pure DOPC, CP/CC 1:1, DOPC/CP 1:1, DOPC/CC 1:1 and DOPC/CP/CC 2:1:1 are shown in Fig. 4 and the characteristic parameters of the films at the collapse point are given in Table 1.

Pure curcumin or cetyl palmitate do not form stable monolayers at the air-water interface. Indeed, pure curcumin is soluble in water, while the hydrophobic cetyl palmitate forms aggregates on the top of the water phase, which are easily observed using Brewster angle microscopy (BAM; results not shown). DOPC shows a typical behavior, consistent with the data reported in the literature [39]. The DOPC monolayer has a liquid-expanded character, with a maximum C_s^{-1} value of 96 mN·m^{-1} (Table 1), a surface area at the collapse of 58 Å^2 and the surface pressure at the collapse of 42 mN·m^{-1}. As expected, BAM images of the DOPC film taken at different surface pressures do not show any anisotropy (results not shown).

The behavior of binary equimolar mixtures with DOPC shows the influence of CC or CP on the DOPC monolayer. For instance, the isotherm of the DOPC/CC 1:1 film is shifted to lower molecular areas compared to pure DOPC, with the A_{coll} value equal to approximately half that of pure DOPC (29 *vs* 58 Å^2). While the profiles of the two isotherms are similar, the compressibility moduli indicate that in the presence of CC the DOPC film is more liquid-like as indicated by the C_{smax}^{-1} values (Fig. 4, inset).

These observations suggest that only small amounts of CC are present in the film formed with DOPC. BAM images (Fig. 5) show that the mixed DOPC/CC 1:1 film is isotropic at low surface pressures (Fig. 5A, B), while some anisotropy of the monolayer appearing at the surface pressure of 37 mN m^{-1} indicates the presence of rare aggregates (Fig. 5C). The morphology of the film after the collapse point, consisting of numerous small aggregates, is well seen (Fig. 5D).

In the case of the DOPC/CP 1:1 film, the slope of the isotherm is steeper compared to pure DOPC and the C_{smax}^{-1} is higher (Fig. 4, inset) indicating that this mixture forms a more rigid, liquid condensed film compared to pure DOPC. The A_{coll} value in the mixed DOPC/CP 1:1 film is low (28 Å^2) compared to pure DOPC (58 Å^2). This effect suggests that the hydrophobic chains of CP molecules may interdigitate with the chains of DOPC inducing condensation of the film forming molecules. Formation of aggregates by CP is possible as well. The latter hypothesis is supported by Brewster angle microscopy (BAM) snapshots showing that the DOPC/CP film is anisotropic all along the compression, with characteristic vegetal-like motifs evoking tree bark and small branches (Fig. 5E-H).

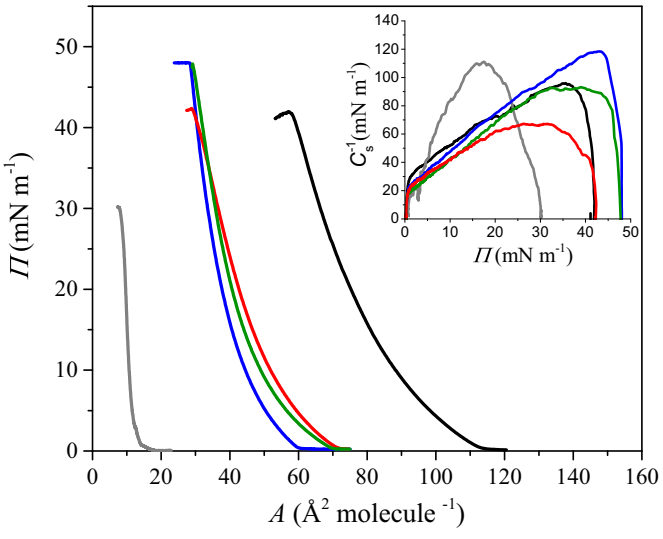

Fig. 4. Π-A compression isotherms. Pure DOPC (black), DOPC/CC 1:1 (red), DOPC/CP/CC 2:1:1 (green), DOPC/CP 1:1 (blue) and CP/CC 1:1 (gray) film spread on water at 25 °C. Inset: C_s^{-1}-Π dependency determined from the experimental isotherms.

Table 1
Compression isotherm parameters at collapse of DOPC, CP/CC (1:1), DOPC/CP (1:1), DOPC/CC (1,1) and DOPC/CP/CC 2:1:1 monolayers at 25 °C.

Monolayers	A_{coll} (Å^2 molecule^{-1})	Π_{coll} (mN m^{-1})	C_{smax}^{-1} (mN m^{-1})
DOPC	57.7	41.8	96
DOPC/CC	29.4	42.0	67
DOPC/CP	28.4	48.0	118
CP/CC	7.9	29.9	111
DOPC/CP/CC	29.2	47.9	93

The CP/CC 1:1 mixture forms a film at the air-water interface. This observation is important, as none of the two pure molecules does. It can be observed that the A_{coll} value of 9 Å^2 is lower than this which could be expected for a mixture containing the two-chain CP. In this situation it is reasonable to suppose that aggregates form in the CP/CC film. BAM images of the mixed CP/CC films show a gas – liquid expanded phase transition at surface pressure close to 0 mN m^{-1} (Fig. 5I). The monolayer shows anisotropy upon compression (Fig. 5J) indicating phase transition, or formation of aggregates. At higher surface pressures the film becomes isotropic (Fig. 5K) indicating, on the contrary, absence of aggregates. The aggregates appear again above the collapse pressure as shown by the presence of bright spots (Fig. 5L). Interestingly, the isotherm of a ternary DOPC/CP/CC 2:1:1 mixture is situated between those corresponding to the DOPC/CP 1:1 and DOPC/CC 1:1 films. It should be noted that the DOPC/CP/CC 2:1:1 film shows anisotropy all along the compression as observed with BAM (results not shown).

Overall, taking into account the results obtained with surface pressure measurements and with BAM, we propose that the CP and CC molecules present in the mixed films containing DOPC interact and undergo a rearrangement at the air-water interface upon compression; CC stabilizes the layer by interacting with CP in the region of the DOPC polar heads.

3.2. Compression isotherms and Brewster angle microscopy of ternary mixtures

To gain further insight into the effect of DOPC on equimolar mixtures of CP and CC, Langmuir isotherms of ternary mixtures were recorded at three different temperatures. The Π-A isotherms of ternary films with different mole fractions of DOPC and 1:1 CP/CC are shown in Fig. 6.

For all systems studied, the surface pressure isotherms of the mixed films are situated between those corresponding to pure DOPC and 1:1 CP/CC monolayers. The increase of DOPC mole fraction results in a shift of the isotherms towards higher molecular areas. The Π_{coll} values of the mixed films depend on the monolayer composition. At 25 °C, the highest Π_{coll} values are found for $x_{DOPC} = 0.4$ and 0.5 around 47 mN·m^{-1}. It should be pointed out that these values are higher compared to those of pure DOPC (42 mN·m^{-1}) or of CP/CC binary mixture (30 mN·m^{-1}). This observation indicates a higher stability of mixed films compared to monolayers spread with pure DOPC or CP/CC 1:1. The same trend is observed at 18 °C and 32 °C with maximum values at $x_{DOPC} = 0.4$ (49 mN·m^{-1}) and 0.2–0.3 (47 mN·m^{-1}), respectively.

It can be observed that for each investigated temperature some Π-A isotherms at high ratio of DOPC show a conspicuous kink in the region 70–80 Å^2 (Fig. 6). The kinks usually interpreted in the literature as phase transition indicate a change of the structure of the films. This change depends on x_{DOPC} and on temperature.

The BAM images (Fig. 7) are shown only for the monolayer corresponding to the DOPC/CP/CC mixture with x_{DOPC} 0.6 at 32 °C, because

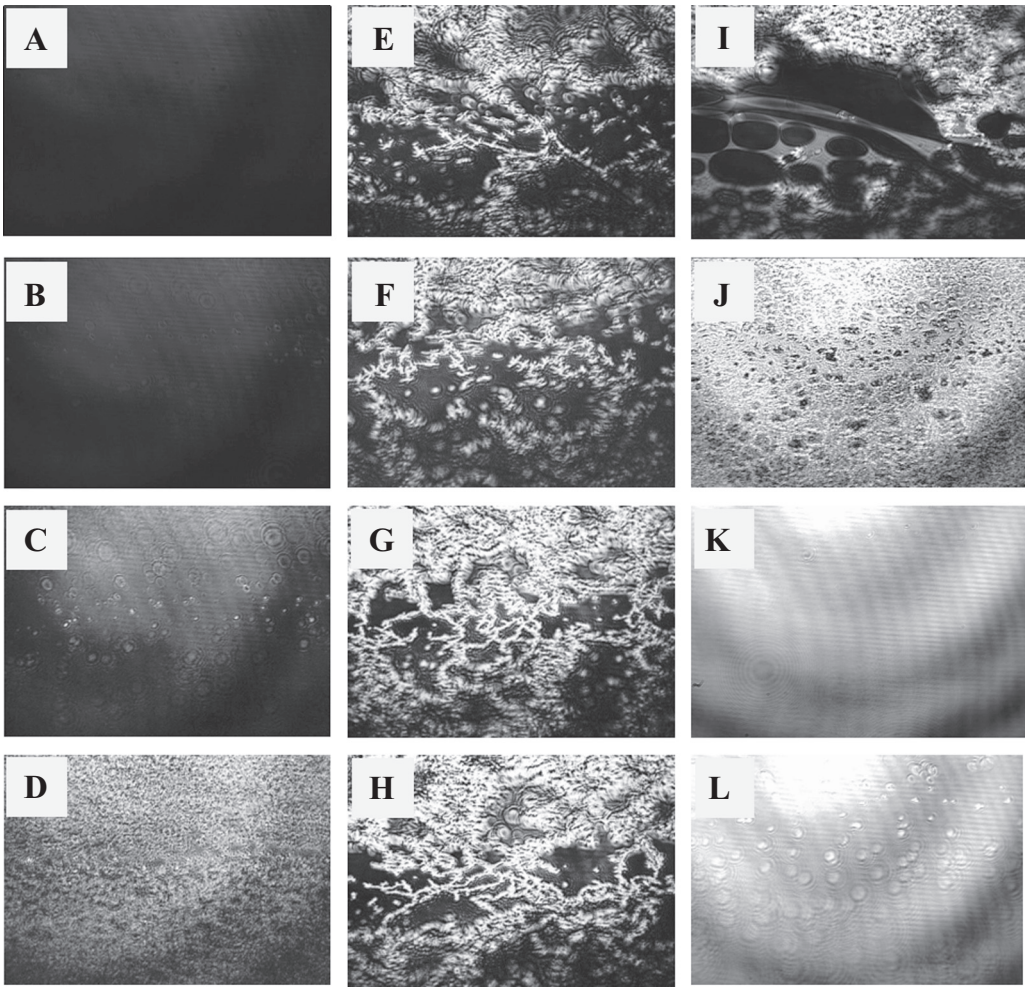

Fig. 5. BAM micrographs of binary mixture of DOPC/CC 1:1, DOPC/CP 1:1 and CP/CC 1:1 at 25 °C. DOPC/CC 1:1 (A–D); DOPC/CP 1:1 (E–H); CP/CC 1:1 (I–L); The images were taken at: Π (mN m^{-1}) = 0 (I), 10 (J), 37 (K), after collapse (L); 0 (E), 10 (F), 30 (G), 40 (H); 0 (A), 5 (B), 23 (C), after collapse (D).

the kink showing at 10 mN m^{-1} is more easily observed compared to the other isotherms. It can be seen that at low surface pressure the structure of the film does not show any anisotropy (Fig. 7A) while at 10 mN m^{-1} bright spots appear (Fig. 7B) which may correspond to a new phase. The spots become brighter and more numerous at 20 mN m^{-1} (Fig. 7C).

In Fig. 8 mean molecular area (MMA) values in the ternary DOPC/CP/CC films are presented as a function of temperature at surface pressure of 10 mN m^{-1}. The latter value was chosen, because a conspicuous kink can be observed at this surface pressure in the isotherms corresponding to the mixtures with high DOPC content (Fig. 6). For all three temperatures the MMA-x_{DOPC} dependencies are approximately linear in the range x_{DOPC} = 0.0–0.5. This effect indicates lack of interaction between molecules and suggest that in this range immiscible phases can coexist. In the range x_{DOPC} = 0.5–1.0 the MMA-x_{DOPC} dependencies are not linear anymore which shows interaction between molecules and may indicate miscibility of the components in the film. These observations are in accordance with those presented in Figs. 6 and 7. It can be

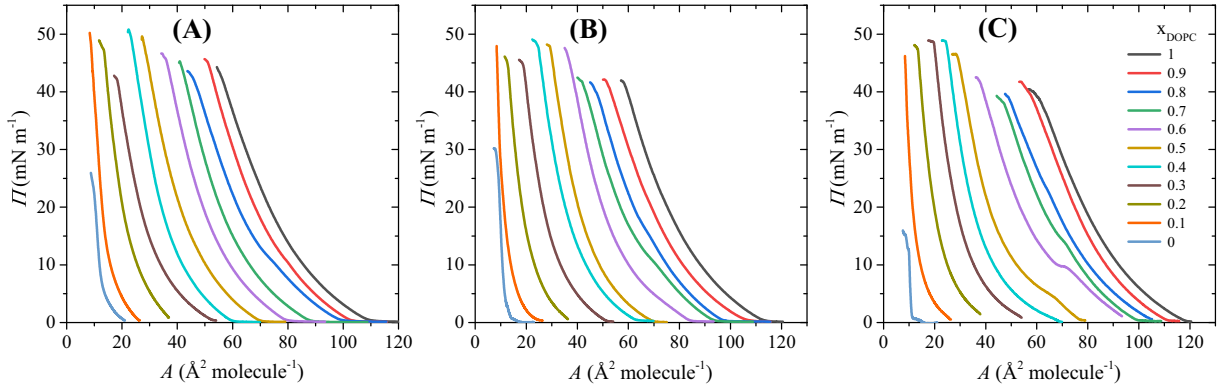

Fig. 6. Π-A isotherms of ternary DOPC/CP/CC mixtures at 18 (A), 25 (B) and 32 °C (C) spread on pure water subphase. Color code: – x_{DOPC} = 1, – 0.9, – 0.8, – 0.7, – 0.6, – 0.5, – 0.4, – 0.3, – 0.2, – 0.1, – 0.

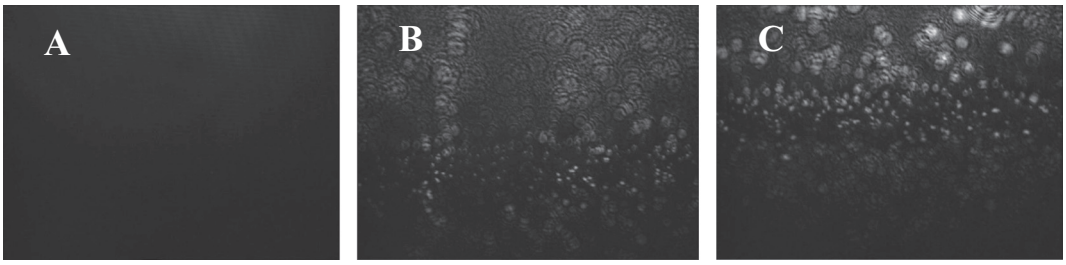

Fig. 7. BAM images for the ternary DOPC/CP/CC mixture with x_{DOPC} 0.6 at 32 °C at different surface pressures. A: 0–1 mN m^{-1}; B: 10 mN m^{-1}; C: 20 mN m^{-1}.

observed that deviation from the additivity of MMA increases with temperature (Fig. 8).

3.3. Thermodynamic analysis of DOPC, CP and CC miscibility in Langmuir layers

The analysis of thermodynamic functions of the multiphase and multicomponent system cannot be performed precisely. Still, the results obtained for Gibbs free energy of mixing (ΔG) suggest the existence of a miscibility gap in the system, depending on temperature.

Based on the results discussed above, it can be proposed that for x_{DOPC} = 0.0–0.4 (32 °C; Fig. 9, red line), a mixture of CP/CC adducts forming aggregates and DOPC molecules accommodated between them forms one phase, as indicated by ΔG = 0; this means ideal miscibility of CP/CC aggregates with DOPC molecules forming the layer. Between 0.4 and 0.8 the phospholipid does not hold in the existing structure any more, as seen in the increasing ΔG, which indicates that phase splitting occurs. Between 0.8 and 1.0 the CP/CC adducts and DOPC molecules form one phase mixed film (ΔG = 0), as the aggregates fall apart. For lower temperatures (18 °C, Fig. 9, blue line) the transition from the CP/CC aggregate-DOPC molecules phase to the mixed CP/CC-DOPC monomolecular film occurs in a continuous way. In this process, CC would influence the aggregation of CP by forming adducts with CP and increasing the polarity of its polar head.

3.4. Molecular dynamics of CP-CC interaction

The side views (*xz* cuts) of monolayers formed with all investigated models at the water-vacuum interface in (N, T, p_n, γ = 20 mN m^{-1}) ensemble are shown in Fig. 10. The width in *y*-direction is equal to 10 Å. It can be seen that chains are the most ordered in the mixed DOPC/CP monolayers. Moreover, in the DOPC/CC monolayers CC molecules are located at the interface, while in CP/CC monolayers they are shifted to the water phase. The pictures corresponding to keto and enol forms of CC are qualitatively similar. Compared to the pure DOPC monolayer (Fig. 10A), CC introduces disordering in DOPC chains (Fig. 10C and D).

The qualitative observation derived from side view plots can be justified by partial density plots presented in Fig. 11. The density profiles are symmetric; therefore, only upper monolayers are shown. In all panels a cyan color corresponds to water. In a case of DOPC, a plot typical for lipids is observed (Fig. 11A). Namely, the terminal methyl groups (dark blue color) are directed towards vacuum and the headgroups are immersed in water (PO_4 - red line and $N(CH_3)_3$ - magenta line). Moreover, the hydrocarbon chain sp^2 carbon atoms located between terminal methyl and PO_4 or choline groups are highlighted in blue. Such qualitative picture of DOPC components is preserved in the two-component DOPC/CP system. The CH_3 (solid dark blue line), PO_4 (red), choline (magenta), and double bond carbon atoms (blue) are less intensive due to lower concentration of DOPC in the monolayer (x_{DOPC} = 0.5). The terminal CH_3 groups of CP (broken dark blue line) coincide with methyl terminal groups of DOPC. The CP oxygen atoms are located at the interface. Carbonyl oxygen atoms (gray area) are slightly shifted left compared to —O— oxygen atoms (black line). A higher ordering of DOPC/CP monolayers compared to those formed with DOPC is manifested by the monolayer thickness, estimated from the positions of terminal methyl and choline groups. The thickness of DOPC monolayer is equal to 21.1 Å, while the DOPC/CP monolayer is equal to 24.3 Å. Interestingly, the presence of CC molecules in the DOPC (Fig. 11C and D) monolayer has no effect on the monolayer thickness which is equal to 21.0 Å and 20.9 Å for enol and keto forms, respectively. All curcumin oxygen atoms (violet ant green lines), are located between PO_4 (red lines) and carbon atoms of double bonds (blue lines). The brown area, black line and

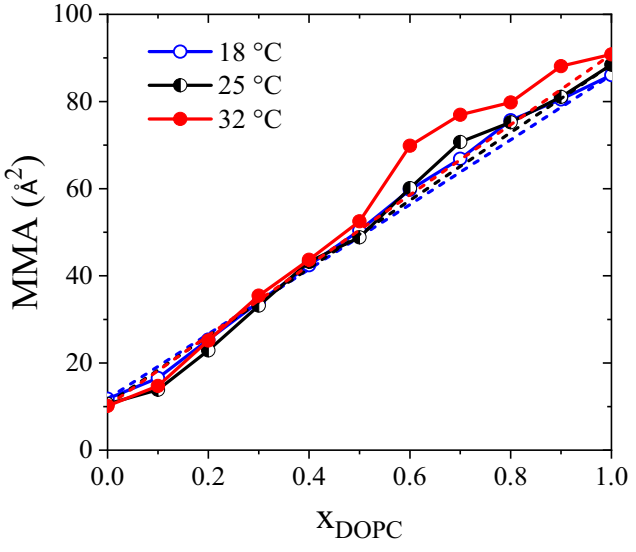

Fig. 8. Mean molecular areas of ternary DOPC/CP/CC films at 18 (○), 25 (◐) and 32 °C (●) and Π = 10 mN·m^{-1} as a function of x_{DOPC}. The straight lines represent the additive mixing.

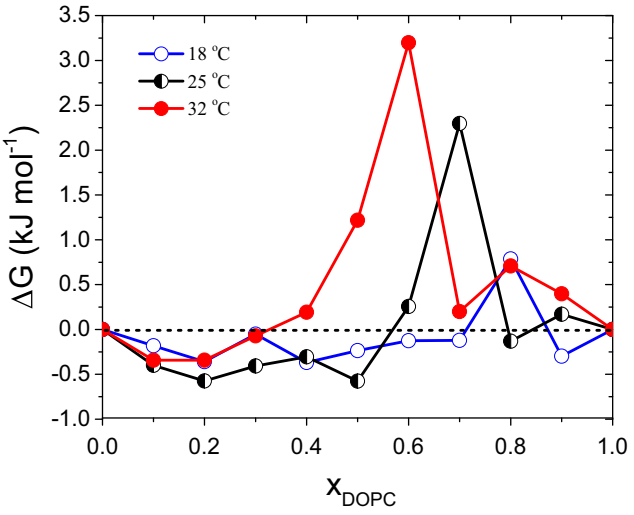

Fig. 9. Thermodynamic analysis of ternary DOPC/CP/CC at 18 °C (○);25 °C (◐) and 32 °C (●) films as a function of x_{DOPC}. Π = 10 mN m^{-1}.

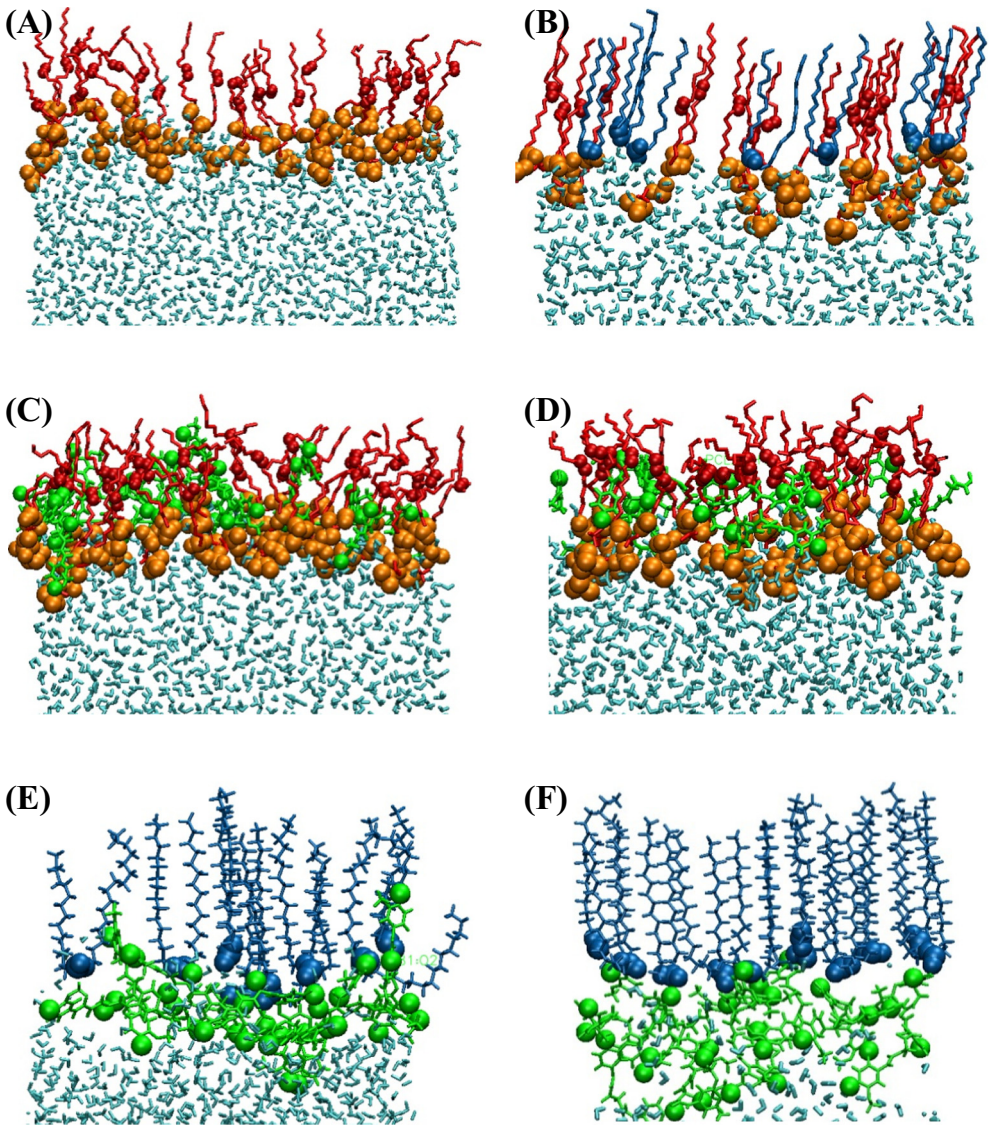

Fig. 10. Side views of DOPC (A), DOPC/CP 1:1 (B), DOPC/CC 1: 1 (C, D) and CP/CC 1:1 (E, F) monolayers. The enol form of CC is shown in panels C and E and the keto form in panels D and F. Color code: red lines – hydrophobic chains of DOPC; blue lines – hydrophobic chains of CP; green lines – curcumin molecule; red balls – carbon atoms of double bonds in DOPC chains; orange balls – hydrophilic headgroups of DOPC; blue balls – hydrophilic headgroups of CP; green balls – hydroxyl oxygens of CC.

green line correspond to hydroxyl, ether and carbonyl oxygens, respectively. These distributions are relatively broad. Quite different behavior of curcumin is observed in the CP/CC systems. Here, the maxima of curcumin oxygen atoms are shifted left compared to CP headgroups (Fig. 11E and F).

The side chain orientation of the DOPC and CP molecules is shown in Fig. 12. Panels A and B correspond to the tilt angle probability distribution of *sn*-1 chain of DOPC and –O-R_1 chain of CP, respectively. The plots for *sn*-2 chain of DOPC and –(C═O)-R_2 of CP show qualitatively the same behavior and are not reported in the paper. Tilt angle is defined by the first and the last chain's carbon atom. Tilt angle probability distribution of *sn*-1 chain in DOPC monolayer (black line) is asymmetric, with the most probable value close to 22°. The presence of CP molecules in the monolayer (red line) increases the phospholipid chain ordering. The distribution becomes narrower, the maximum is shifted towards lower value and the probability is twice as high as previously observed for one-component monolayer. In contrast to CP, the presence of CC has a small disordering effect on the lipid chain orientation. The influence of both forms of curcumin (blue and green lines) on chain ordering is similar. The most probable values are shifted right towards higher values, probability distributions are more diffused and symmetric as compared to one-component monolayer. Small disordering effect of CC keto (green line) and enol (blue line) forms on CP chains can also be observed (Fig. 12B). The curves are now shifted left towards smaller angles. Both probability distributions are more diffused. However, CP chains are more ordered compared to DOPC and DOPC/CC systems.

The hydration of the ester C═O groups is shown in Fig. A1 in the Supplementary Materials. The carbonyl ester groups are present in DOPC and CP molecules. The highest hydration is observed for the ester carboxyl oxygens in the two-component DOPC/CP monolayer. Hydration of the ester carbonyl oxygen in CP is higher compared to DOPC. The CP headgroups are easily penetrable by water due to the small size (see Fig. 10B). The presence of the small CP headgroups increases water accessibility to DOPC carbonyl groups. Hydration of carbonyl oxygens in DOPC/CC enol or DOPC/CC keto is comparable and only slightly smaller than in the DOPC monolayer. The highest impact of curcumin is observed in the CP/CC systems. Curcumin molecules, whatever the tautomer, significantly reduce hydration of the CP carbonyl oxygens.

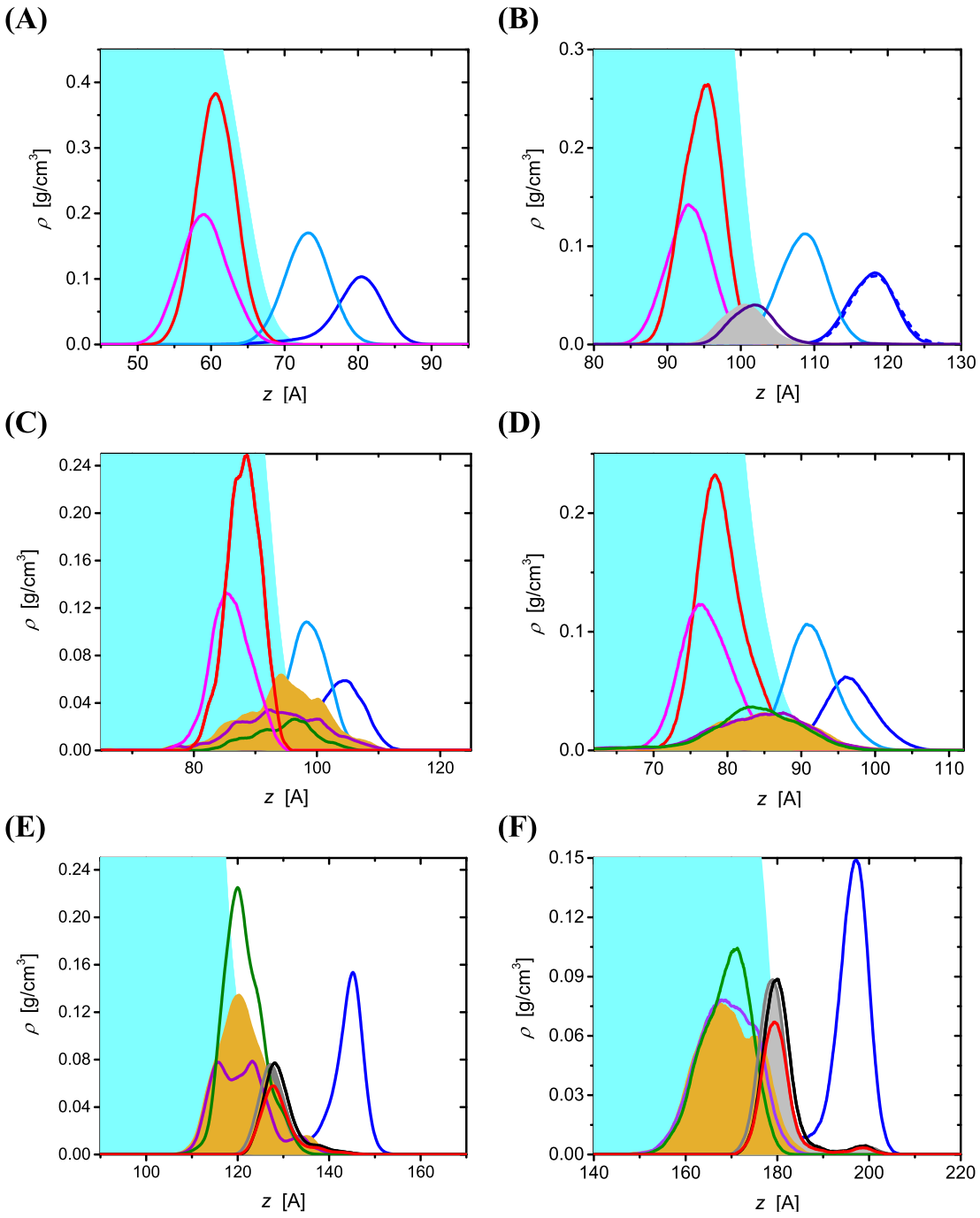

Fig. 11. Density profiles along monolayer normal of DOPC (A), DOPC/CP 1:1 (B), DOPC/CC 1:1 enol form (C), DOPC/CC 1:1 keto form (D), CP/CC 1:1 enol form (E) and CP/CC 1:1 keto form (F). Color code: cyan area – water phase, dark blue line – terminal methyl groups, blue line – double bonds in DOPC side chains, red line – PO_4, magenta line – choline groups, gray area – carbonyl oxygen atoms in CP, black line —O— in CP, brown area – hydroxyl oxygen atoms in CC, violet line – ether oxygen atoms in CC, green line – carbonyl oxygen atoms in CC. Dark broken line – terminal methyl group in CP in the DOPC/CP system.

3.5. PM-IRRAS of the monomolecular films

The results obtained for pure DOPC, mixed DOPC/CP 1:1, DOPC/CC 1:1 and DOPC/CP/CC 2:1:1 monolayers at $\Pi = 30$ mN m^{-1} are presented in Table 2 and in Fig. A2.

The symmetric and asymmetric methylene stretching vibration, as well as the carbonyl stretching vibrations are clearly visible in the spectra. The wavenumbers of methylene stretching vibration were used to monitor the degree of conformational ordering of the alkyl chains in the molecules [40,41]. The $\nu_{as}(CH_2)$ and $\nu_s(CH_2)$ bands of mixed DOPC/CP monolayers show at 2918 and 2850 cm^{-1}, respectively, indicating an *all-trans* arrangement of the hydrocarbon chains. Upon adding curcumin to the DOPC or DOPC/CP monolayers, the bands shift towards higher wavenumbers, suggesting chain disordering (*gauche* conformers). Concerning the DOPC ester group, the shift of the stretching ν(C═O) band to lower wavenumbers indicates that a higher number of carbonyl groups is hydrogen bonded [42,43]. The lower frequencies of the carbonyl stretching bands for the ester groups should be associated to higher hydration of the ester groups but also to their interaction with CC. It has to be mentioned that the CP and DOPC ester bands cannot

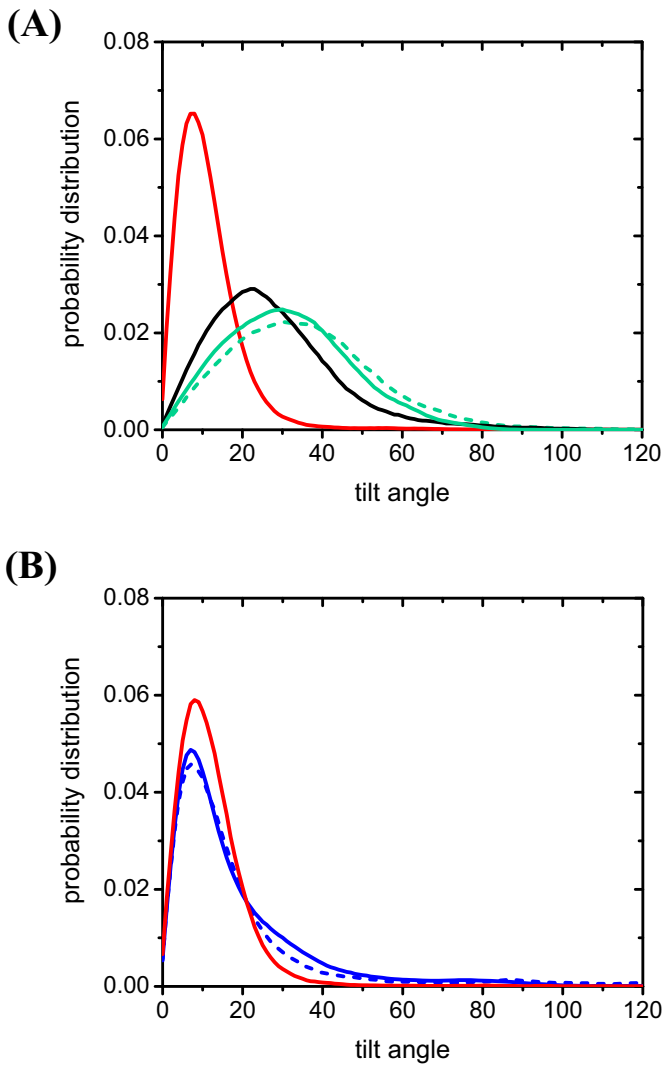

Fig. 12. Tilt angle probability distribution of *sn*-1 chain of DOPC (A) and –O-$C_{16}H_{33}$ chain of CP (B). Color code: DOPC – black, DOPC/CP – red, DOPC/CC – green, CP/CC blue. The solid and broken lines correspond to enol and keto isomers of curcumin, respectively.

be distinguished in the spectra. Nevertheless, as indicated by the ν(C═O) wavenumber value of 1730 cm^{-1} (Table 2), the hydration of the ester groups in the DOPC/CP is the highest compared to the other films. The presence of CC molecules in the film affects slightly the position of the CO stretching bands. Indeed, a small blueshift of the ν(C═O) is observed in DOPC/CC and DOPC/CP/CC, compared to pure DOPC or mixed DOPC/CP monolayers, respectively. These results suggest a reduced hydration of the DOPC carbonyl group in the presence of curcumin in the film. This effect may be due to hydrocarbon chain disordering in the presence of CC and, consequently, perturbation of the hydrogen network within the polar head region. It should be noted that the PM-IRRAS results are in accordance with those obtained with molecular modeling. The latter show that CC significantly reduces hydration of the CP carbonyl oxygens; such interaction was not observed in the case of DOPC.

Table 2
Assignment of the main vibration bands in pure DOPC and in the presence of CP or/and CC at 30 mN m^{-1}. Temperature: 25 °C.

Monolayer	ν_{as} (CH_2) (cm^{-1})	ν_s (CH_2) (cm^{-1})	ν (C═O) (cm^{-1})
DOPC	2933	2845	1734
DOPC/CP	2918	2850	1730
DOPC/CC	2935	2861	1736
DOPC/CP/CC	2923	2851	1735

4. Conclusions

This study showed that the effect of curcumin on model membranes formed at the air-water interface with DOPC is intensified by the presence of cetyl palmitate in the lipid film. Based on the results obtained with compression isotherms, we propose that CP and CC molecules present in the mixed films containing DOPC interact and undergo a rearrangement at the air-water interface upon compression; CC stabilizes the lipid layer by interacting with CP in the region of the DOPC polar heads. Molecular dynamics support this proposal by demonstrating that CC molecules are located in the lipid layer formed with DOPC/CC, while in the CP/CC system they are displaced to the aqueous region of the CP polar heads. CC molecules, independently of the form of the isomer, significantly reduce hydration of the CP carbonyl oxygens. The effect of an increased hydrogen bonding of carbonyl groups demonstrated with PM-IRRAS in the monomolecular films containing CC is in accordance with the latter effect demonstrated with molecular dynamics. Moreover, both methods showed that curcumin induces chain disordering in the DOPC or DOPC/CP monolayers.

Thermodynamic analysis indicates different miscibility of the systems, depending on the temperature. We propose that at 32 °C, ideal miscibility of CP/CC aggregates with DOPC occurs in function of x_{DOPC}, followed by phase splitting and formation of one phase composed of CP/CC adducts and DOPC molecules, as the aggregates fall apart. At lower temperatures (18 °C) the transition from the CP/CC aggregate-DOPC phase to the mixed CP/CC-DOPC monomolecular film follows in a continuous way. In this process, CC would influence aggregation by forming adducts with CP and increasing the polarity of its polar head.

A better understanding of the molecular interaction obtained in this study may be of interest for developing lipid systems for introducing curcumin into lipid membranes and transporting it into living cells.

CRediT authorship contribution statement

Maxime Girardon: Investigation.**Beata Korchowiec:**Writing - review & editing, Methodology, Data curation.**Jacek Korchowiec:**Software, Formal analysis, Writing - original draft.**Ewa Rogalska:** Conceptualization, Writing - review & editing.**Nadia Canilho:**Resources, Validation.**Andreea Pasc:**Supervision, Funding acquisition.

Declaration of competing interest

The authors declare that they have no known competing financial interests or personal relationships that could have appeared to influence the work reported in this paper.

Acknowledgments

M.G. acknowledges the French Ministry for Research and Education for the PhD grant and S. Parant for technical assistance on the PhotoNS characterization platform. NC and AP acknowledge financial support through the “Fire Light” project (Photo-Bio-Actifs Molecules and Nanoparticles), co-funded by the European Union under the program “FEDER-FSE Lorraine et Massif des Vosges 2014–2020”. The calculations were carried out on the PL-Grid infrastructure at ACK CYFRONET.

Appendix A. Supplementary data

Supplementary data to this article can be found online at https://doi.org/10.1016/j.molliq.2020.113040.

References

[1] A. Marchiani, C. Rozzo, A. Fadda, G. Delogu, P. Ruzza, Curr. Med. Chem. 21 (2014) 204.
[2] S.C. Gupta, B. Sung, J.H. Kim, S. Prasad, S. Li, B.B. Aggarwal, Mol. Nutr. Food Res. 57 (2013) 1510.
[3] P. Anand, A.B. Kunnumakkara, R.A. Newman, B.B. Aggarwal, Mol. Pharm. 4 (2007) 807.
[4] B.B. Aggarwal, B. Sung, Trends Pharmacol. Sci. 30 (2009) 85.
[5] H. Chen, J. Wu, M. Sun, C. Guo, A. Yu, F. Cao, L. Zhao, Q. Tan, G. Zhai, J. Liposome Res. 22 (2012) 100.
[6] M. Girardon, S. Parant, A. Monari, F. Dehez, C. Chipot, E. Rogalska, N. Canilho, A. Pasc, ChemPhotoChem 3 (2019) 1034.
[7] J. Cui, B. Yu, Y. Zhao, W. Zhu, H. Li, H. Lou, G. Zhai, Int. J. Pharm. 371 (2009) 148.
[8] M. Sharma, S. Sharma, J. Wadhwa, Artif. Cells, Nanomed., Biotechnol. 47 (2019) 45.
[9] A. Beloqui, P.B. Memvanga, R. Coco, S. Reimondez-Troitino, M. Alhouayek, G.G. Muccioli, M.J. Alonso, N. Csaba, M. de la Fuente, V. Preat, Colloids Surf., B 143 (2016) 327.
[10] N.M. Khalil, T.C. Frabel do Nascimento, D.M. Casa, L.F. Dalmolin, A.C. de Mattos, I. Hoss, M.A. Romano, R.M. Mainardes, Colloids Surf., B 101 (2013) 353.
[11] Y. Gao, S. Ding, X. Huang, Z. Fan, J. Sun, Y. Hai, K. Li, Drug Dev. Ind. Pharm. 45 (2019) 273.
[12] S. Kim, R. Diab, O. Joubert, N. Canilho, A. Pasc, Colloids Surf., B 140 (2016) 161.
[13] S. Kim, M.-J. Stebe, J.-L. Blin, A. Pasc, J. Mater. Chem. B 2 (2014) 7910.
[14] S. Mukherjee, S. Ray, R.S. Thakur, Indian J. Pharm. Sci. 71 (2009) 349.
[15] J.K. Seydel, E.A. Coats, H.P. Cordes, M. Wiese, Arch. Pharm. (Weinheim, Ger.) 327 (1994) 601.
[16] C. Stefaniu, G. Brezesinski, H. Moehwald, Adv. Colloid Interf. Sci. 208 (2014) 197.
[17] K. Czapla, B. Korchowiec, M. Orlof, J.R. Magnieto, E. Rogalska, J. Phys. Chem. B 115 (2011) 9290.
[18] B. Korchowiec, M. Gorczyca, K. Wojszko, M. Janikowska, M. Henry, E. Rogalska, Biochim. Biophys. Acta Biomembr. 1848 (2015) 1963.
[19] J. Gravier, B. Korchowiec, R. Schneider, E. Rogalska, Chem. Phys. Lipids 158 (2009) 102.
[20] B. Korchowiec, M. Gorczyca, E. Rogalska, J.-B. Regnouf-de-Vains, M. Mourer, J. Korchowiec, Soft Matter 12 (2016) 181.
[21] K. Sabatini, J.-P. Mattila, F.M. Megli, P.K.J. Kinnunen, Biophys. J. 90 (2006) 4488.
[22] M.E. Mariani, M.E. Sanchez-Borzone, D.A. Garcia, Chem. Phys. Lipids 198 (2016) 39.
[23] M.J. Sanchez-Martin, I. Haro, M.A. Alsina, M.A. Busquets, M. Pujol, J. Phys. Chem. B 114 (2010) 448.
[24] V. Teeranachaideekul, E.B. Souto, V.B. Junyaprasert, R.H. Mueller, Eur. J. Pharm. Biopharm. 67 (2007) 141.
[25] J.T. Davies, E.K. Rideal, Interfacial Phenomena, 2nd ed Academic Press, New York-London, 1963.
[26] F.C. Goodrich, Proc. Int. Congr. Surf. Act., 2nd 1 (1957) 85.
[27] K.J. Bacon, G.T. Barnes, J. Colloid Interface Sci. 67 (1978) 70.
[28] B. Korchowiec, M. Gorczyca, A.B. Salem, J.-B. Regnouf de Vains, E. Rogalska, Colloids Surf. B: Biointerfaces 103 (2013) 217.
[29] W. Schulte, M. Orlof, I. Brand, B. Korchowiec, E. Rogalska, Colloids Surf. B: Biointerfaces 116 (2014) 389.
[30] D. Blaudez, J.-M. Turlet, J. Dufourcq, D. Bard, T. Buffeteau, B. Desbat, J. Chem. Soc. Faraday Trans. 92 (1996) 525.
[31] S. Grimme, J. Comput. Chem. 27 (2006) 1787.
[32] M.J. Frisch, G.W. Trucks, H.B. Schlegel, G.E. Scuseria, M.A. Robb, J.R. Cheeseman, G. Scalami, V. Barone, B. Menucci, G.A. Petersson, H. Nakatsuji, M. Caricato, X. Li, H.P. Hratchian, A.F. Izmaylov, J. Bloino, G. Zheng, J.L. Sonnenberg, M. Hada, M. Ehara, K. Toyota, R. Fukuda, J. Hasegawa, M. Ishida, T. Nakajima, Y. Honda, O. Kitao, H. Nakai, T. Vreven, J.A. Montgomery Jr., J.E. Peralta, F. Ogliaro, M. Bearpark, J. Heyd, E. Brothers, K.N. Kudin, V.N. Staroverov, R. Kobayashi, J. Normand, K. Raghavachari, A. Rendell, J.C. Burant, S.S. Iyengar, J. Tomasi, M. Cossi, N. Rega, J.M. Millam, M. Klene, J.E. Knox, J.B. Cross, V. Bakken, C. Adamo, J. Jaramillo, R. Gomperts, R.E. Stratmann, O. Yazyev, A.J. Austrin, R. Cammi, C. Pomelli, W. Ochterski, R.L. Martin, K. Morokuma, V.G. Zakrzewski, G.A. Voth, P. Salvador, J.J. Dannenberg, S. Dapprich, A.D. Daniels, O. Farkas, J.B. Foresman, J.V. Ortiz, J. Cioslowski, D.J. Fox, Gaussian 09, Revision A.02, Gaussian Inc, Wallingford CT, 2009.
[33] J.B. Klauda, R.M. Venable, J.A. Freites, J.W. O'Connor, D.J. Tobias, C. Mondragon-Ramirez, I. Vorobyov, A.D. MacKerell Jr., R.W. Pastor, J. Phys. Chem. B 114 (2010) 7830.
[34] C.G. Mayne, J. Saam, K. Schulten, E. Tajkhorshid, J.C. Gumbart, J. Comput. Chem. 34 (2013) 2757.
[35] J. Tomasi, B. Mennucci, R. Cammi, Chem. Rev. 105 (2005) 2999.
[36] J.C. Phillips, R. Braun, W. Wang, J. Gumbart, E. Tajkhorshid, E. Villa, C. Chipot, R.D. Skeel, L. Kale, K. Schulten, J. Comput. Chem. 26 (2005) 1781.
[37] W.L. Jorgensen, J. Chandrasekhar, J.D. Madura, R.W. Impey, M.L. Klein, J. Chem. Phys. 79 (1983) 926.
[38] W. Humphrey, A. Dalke, K. Schulten, J. Mol. Graph. 14 (1996) 33.
[39] C. Hao, R. Sun, J. Zhang, Colloids Surf., B 112 (2013) 441.
[40] B. Korchowiec, Y. Corvis, T. Viitala, C. Feidt, Y. Guiavarch, C. Corbier, E. Rogalska, J. Phys. Chem. B 112 (2008), 13518.
[41] R.A. MacPhail, H.L. Strauss, R.G. Snyder, C.A. Elliger, J. Phys. Chem. 88 (1984) 334.
[42] J.M. Vanderkooi, J.L. Dashnau, B. Zelent, Biochim. Biophys. Acta, Proteins Proteomics 1749 (2005) 214.
[43] K. Czapla, B. Korchowiec, M. Orlof, J.R. Magnieto, E. Rogalska, J. Phys. Chem. B 115 (2011) 9290.